PHYSICAL REVIEW A VOLUME 4, NUMBER 2 AUGUST 1971

Production of Carbon K X Rays by Heavy-Ion Bombardment*

R. C. Der, R. J. Fortner, T. M. Kavanagh, and J. M. Khan
Lawrence Radiation Laboratory, University of California, Livermore, California 94550
(Received 15 January 1971)

Cross sections for K x-ray production in carbon are presented for collisions involving incident C^+, N^+, O^+, Ne^+, Ar^+, Kr^+, and Xe^+ in the energy range 20 keV–1.5 MeV. Thick-target x-ray yield data are also included. The cross-section measurements are in excellent agreement with a simple theoretical model based on the Landau-Zener theory of level crossing.

I. INTRODUCTION

It is well known that in ion-atom collisions inner-shell vacancies can be created with high probability even at collision energies for which velocities are small compared to the velocities of the inner-shell electrons involved. We have discussed carbon K-shell vacancy production in such collisions in several earlier papers.[1-3] Cross sections were shown to be very large—essentially geometric at energies above about 10 keV per atomic mass unit for the incident particles. The data were interpreted in terms of a model proposed by Fano and Lichten[4] in which the excitation mechanism depends on an interpenetration of the atomic shells of the projectile and the target atom, with the creation of a quasi-molecule; excitations occur at level crossings in this complex dynamic system. The cross-section data were based on measurements of carbon K x rays emitted following the creation of K-shell vacancies in carbon. Complete data, including absolute thick-target x-ray yields, have previously been reported for only the C^+-C case[2]; this paper presents complete data for the other ion-atom systems discussed in Refs. 1 and 3. Data for incident N^+, O^+, Ne^+, Ar^+, Kr^+, and Xe^+ ions are presented, for ion energies in the range 20 keV–1.5 MeV.

Other similar x-ray cross-section measurements for different ion-atom systems have been reported by Specht,[5] Brandt and Laubert,[6] Saris and Onderdelinden,[7] Needham and Sartwell,[8] and Kavanagh *et al.*[9]

II. METHOD AND RESULTS

The experimental techniques have been discussed in Refs. 1 and 2, and in more detail in an earlier paper on proton bombardment of carbon.[10] A thick carbon target was used, and carbon K x rays were detected by a gas-flow proportional counter with a Mylar window. The directly measured quantity was the x-ray counts per unit charge incident upon the target. The absolute thick-target yield for a given heavy ion (x rays emitted from the target surface, per incident ion) was obtained by bombarding the carbon target alternately with protons and the heavy ion, and then normalizing the heavy-ion data to the previously determined thick-target yield for protons.[10] The measurements were made on two separate accelerators. Data from 20 to 120 keV were obtained by using a 120-kV dc power supply and a duoplasmatron ion source. A Van de Graaff accelerator with a conventional rf electrodeless discharge source provided ions in the range 100 keV–1.5 MeV. Only the low-energy accelerator was used for Kr^+ and Xe^+. The various ion beams were obtained by using appropriate gases in the ion source, with magnetic analysis of the beam to isolate the desired ionic component. (The molecular ions O_2^+ and N_2^+ were used in some cases, in order to extend the energy range, and a comparison with O^+ or N^+ data indicated that in the target the molecular ions were equivalent to two O^+ or N^+ ions of half the energy. Some measurements were also made with doubly charged Ne^{++} ions and, to within experimental errors, the results for a given incident ion kinetic energy were shown to be independent of the initial charge state of the ion.)

The experimental data are presented in Table I, and are shown graphically in Figs. 1 and 2. The thick-target yields I are in column 2 of the table, and are plotted as a function of ion energy in Fig. 1. The x-ray production cross section σ_x, in the second to last column of the table, was calculated from the thick-target yield I according to the relation

$$\sigma_x = \frac{dI}{dE} S + \frac{1}{n} \frac{\mu}{\rho} I , \tag{1}$$

where S is the target stopping cross section for the incident ion, n is the number of target atoms per gram, and μ/ρ is the target absorption coefficient for the carbon x rays. The second term in Eq. (1) is not important at low bombarding energies (i.e., target self-absorption is small), but may represent as much as a third of the total cross section at higher energies. The values used for the stopping cross sections are given explicitly in Table I, with the nuclear and electronic parts shown separately. The total stopping cross section S is the sum of these two components. The nuclear component was

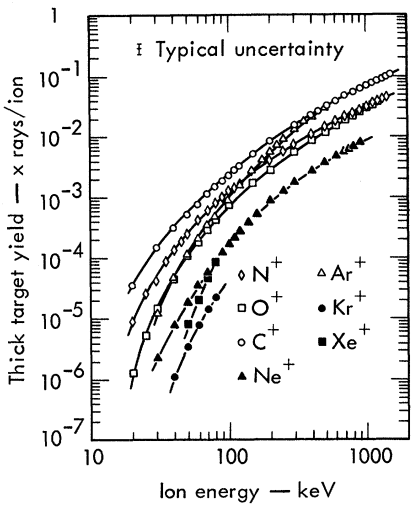

FIG. 1. Experimental thick-target x-ray yields as a function of incident-ion energy. Data for C^+ are from Ref. 2.

calculated from the theory of Lindhard, Scharff, and Schiøtt,[11] and experimental electronic-stopping data were taken from the measurements of Ormrod and Duckworth,[12] Porat and Ramavataram,[13] and Fastrup, Hvelplund, and Sautter.[14] Electronic stopping for Kr^+ and Xe^+ were calculated from Ref. 11. The K-shell excitation cross section σ_I is related to σ_x by

$$\sigma_x = \omega_K \sigma_I \ , \tag{2}$$

where ω_K is the K-shell fluorescence yield, taken to be 0.00113.[15] (This more recent value is larger than that used in our earlier papers.[1-3] It should be noted in this regard that conventional fluorescence-yield values *may not* apply to these complex interactions in which considerable outer-shell excitation is expected; in solid targets, however, outer-shell relaxation probably occurs fast enough to make this an unimportant consideration, except, perhaps, for the moving carbon ion in the C^+-C case.) Values of σ_I are in the last column of the table and are plotted in Fig. 2 as a function of incident-ion energy per atomic mass unit. Data for C^+-C from Ref. 2 are included, for completeness, in Figs. 1 and 2. (The data for C^+-C in Fig. 2 differ slightly from Ref. 2 because of the different value used here for the fluorescence yield.) Figure 2 also shows data for incident protons, taken from Ref. 10, and corrected to incorporate better stopping cross-section[12,16] and fluorescence-yield[15] data; the proton data are considered to be representative of collisions involving direct Coulomb excitation. The experimental uncertainty in the present data is estimated to be ~15% for I and ~30% for σ_x, except for the Ar^+-C case, for which the uncertainty is somewhat larger (see the following paragraph).

Values for σ_I have an additional uncertainty due to uncertainty in the fluorescence yield, and the error quoted[15] for ω_K leads to a standard error of about 35% for σ_I. The relative error for points on a given cross-section curve is about 15%.

It should be noted that vacancies will be produced in the incident ions as well as in carbon target atoms, and x rays from the incident ions may be registered by the detector. This is certainly the case for the C^+-C system, in which both ion and atom contribute to the measured yield of carbon K x rays. The use of Mylar (essentially carbon) windows on the proportional counter provided a convenient critical absorber (K edge 284 eV) for eliminating or reducing effects due to other projectile x rays that could not be distinguished from carbon K x rays by pulse-height analysis alone. The windows were $\frac{1}{4}$–$\frac{3}{4}$ mm thick, and the thinnest windows had ~5% transmission for carbon K x rays, ~0.25% for "normal"[17] (~220 eV) argon L x rays, and negligible transmission for K x rays of nitrogen and oxygen, M x rays of krypton, and N x rays of xenon. Discrimination against unwanted x rays is, of course, even more effective for the thicker windows. Some uncertainty exists, however, in the effectiveness of this discrimination for the Ar^+-C system, since it has recently been shown[17] that in Ar^+-Ar collisions outer-shell excitation of argon can lead to the production of L x-ray components of higher than normal energies—in some cases even higher than ground-state L edges. Such energy shifts for argon L x rays produced in Ar^+-C collisions would, of course, lead to their increased transmission through the counter window. Preliminary spectroscopic measurements using diffraction

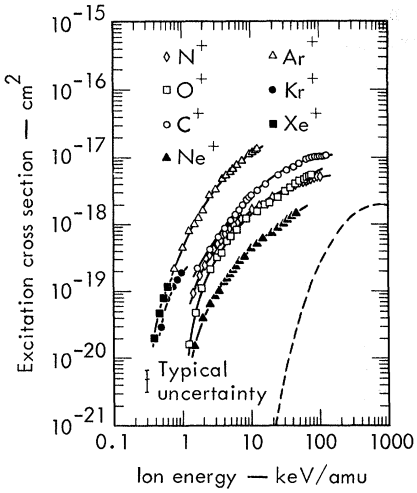

FIG. 2. Carbon K-shell excitation cross sections as a function of incident-ion energy per amu. Data for C^+ are from Ref. 2. The dashed curve is for incident protons, and is taken from Ref. 10.

TABLE I. Experimental results. The tabulated quantities are defined in connection with Eqs. (1) and (2) in the text. The stopping cross section $S(E)$ in column 6 is the sum of the electronic and nuclear contributions $S_e(E)$ and $S_v(E)$.

E (keV)	I $\left(10^{-3}\frac{\text{x rays}}{\text{ion}}\right)$	dI/dE $\left(10^{-5}\frac{\text{x rays}}{\text{ion keV}}\right)$	$S_e(E)$ $\left(10^{-17}\frac{\text{keV cm}^2}{\text{atom}}\right)$	$S_v(E)$ $\left(10^{-17}\frac{\text{keV cm}^2}{\text{atom}}\right)$	$S(E)dI/dE$ (10^{-22} cm^2)	$(1/n)(\mu/\rho)I$ (10^{-22} cm^2)	σ_x (10^{-22} cm^2)	σ_I (10^{-18} cm^2)
				Nitrogen				
20[a]	0.009	0.248	2.25	2.1	1.08	0.004	1.08	0.095
25[a]	0.026	0.435	2.52	1.9	1.92	0.01	1.93	0.169
30	0.042	0.608	2.80	1.7	2.74	0.02	2.76	0.244
35[a]	0.089	0.826	3.00	1.6	3.80	0.04	3.84	0.339
40[a]	0.133	1.03	3.15	1.5	4.79	0.06	4.85	0.429
45[a]	0.186	1.22	3.3	1.4	5.76	0.08	5.84	0.516
50	0.242	1.42	3.5	1.3	6.82	0.10	6.92	0.611
60	0.432	1.65	3.8	1.15	8.15	0.19	8.34	0.737
70	0.612	1.86	4.0	1.05	9.40	0.26	9.66	0.851
80	0.802	2.05	4.2	0.98	10.6	0.35	10.9	0.97
90	1.00	2.20	4.4	0.90	11.6	0.43	12.0	1.07
100	1.25	2.35	4.6	0.85	12.7	0.54	13.2	1.16
110	1.41	2.48	4.7	0.80	13.6	0.61	14.2	1.25
120	1.68	2.58	4.8	0.76	14.5	0.73	15.2	1.34
150	2.53	2.84	5.3	0.64	17.1	1.1	18.2	1.61
200	4.05	3.16	5.95	0.56	20.5	1.7	22.2	1.95
250	5.80	3.33	6.5	0.45	23.3	2.5	25.8	2.28
300	7.46	3.33	7.0	0.39	24.6	3.2	27.8	2.46
400	10.8	3.33	7.8	0.34	27.3	4.7	32.0	2.82
500	14.3	3.32	8.6	0.27	29.5	6.2	35.7	3.15
600	17.9	3.32	9.2	0.23	31.5	7.4	38.9	3.43
700	21.3	3.32	9.9	0.20	33.5	9.2	42.7	3.77
800	24.3	3.32	10.5	0.18	35.5	10.5	46.0	4.06
900	27.6	3.32	11.0	0.17	37.5	11.9	49.4	4.36
1000	30.9	3.32	11.7	0.15	39.2	13.3	52.5	4.63
1100	34.3	3.25	12.1	0.14	39.6	14.7	54.3	4.78
1200	37.7	3.07	12.6	0.13	39.0	16.3	55.3	4.88
1300	40.9	2.90	12.9	0.13	37.7	17.7	55.4	4.89
1400	43.7	2.69	13.4	0.12	36.3	18.9	55.2	4.88
				Oxygen				
20[b]	0.0013	0.038	2.2	2.7	0.19	0.0005	0.19	0.017
25[b]	0.0052	0.114	2.4	2.4	0.55	0.001	0.55	0.049
30[b]	0.015	0.256	2.6	2.2	1.23	0.006	1.24	0.110
40	0.044	0.489	2.9	2.0	2.40	0.02	2.42	0.212
50	0.104	0.701	3.25	1.75	3.51	0.05	3.56	0.315
60	0.176	0.813	3.5	1.60	4.15	0.08	4.23	0.373
70	0.287	1.19	3.75	1.45	6.19	0.12	6.31	0.558
80	0.414	1.38	3.95	1.35	7.30	0.20	7.50	0.662
100	0.76	1.66	4.30	1.20	9.15	0.33	9.50	0.838
150	1.71	2.20	5.10	0.92	13.2	0.74	13.9	1.23
200	2.76	2.49	5.70	0.76	16.2	1.20	17.4	1.54
300	5.4	2.82	6.80	0.56	20.9	2.30	23.2	2.05
400	8.6	3.01	7.60	0.46	24.3	3.7	28.0	2.48
500	11.7	3.30	8.35	0.38	28.9	5.1	34.0	3.01
600	15.0	3.42	9.05	0.335	32.1	6.5	38.6	3.42
700	18.5	3.53	9.60	0.295	34.9	8.3	43.2	3.82
800	22.0	3.67	10.2	0.265	38.5	9.5	48.0	4.24
900	25.7	3.58	10.8	0.24	39.4	11.1	50.5	4.47
1000	29.6	3.56	11.4	0.225	41.3	12.8	54.1	4.77
1100	33.0	3.53	11.8	0.205	42.4	14.3	56.7	5.00
1200	36.6	3.53	12.3	0.19	44.1	15.8	59.1	5.22

TABLE I. (*Continued*).

E (keV)	I $\left(10^{-3}\frac{\text{x rays}}{\text{ion}}\right)$	dI/dE $\left(10^{-5}\frac{\text{x rays}}{\text{ion keV}}\right)$	$S_e(E)$ $\left(10^{-17}\frac{\text{keV cm}^2}{\text{atom}}\right)$	$S_v(E)$ $\left(10^{-17}\frac{\text{keV cm}^2}{\text{atom}}\right)$	$S(E)dI/dE$ $(10^{-22}$ cm$^2)$	$(1/n)(\mu/\rho)I$ $(10^{-22}$ cm$^2)$	σ_x $(10^{-22}$ cm$^2)$	σ_I $(10^{-18}$ cm$^2)$
				Neon				
30	0.0022	0.31	1.85	3.6	0.169	0.001	0.17	0.015
40	0.0075	0.0856	2.1	3.2	0.46	0.003	0.46	0.040
50	0.018	0.136	2.4	2.9	0.723	0.01	0.73	0.064
60	0.035	0.178	2.6	2.65	0.935	0.02	0.97	0.086
70	0.568	0.223	2.8	2.40	1.14	0.03	1.17	0.103
80	0.87	0.287	3.0	2.20	1.48	0.04	1.52	0.134
90	0.122	0.330	3.2	2.1	1.75	0.05	1.80	0.159
100	0.163	0.378	3.3	2.0	2.00	0.07	2.07	0.182
110	0.213	0.425	3.4	1.9	2.26	0.09	2.35	0.208
120	0.261	0.470	3.6	1.8	2.54	0.11	2.65	0.234
140[c]	0.367	0.555	3.9	1.6	3.05	0.16	3.20	0.282
160[c]	0.522	0.628	4.1	1.5	3.52	0.22	3.74	0.330
200[c]	0.863	0.78	4.5	1.3	4.53	0.33	4.85	0.429
250	1.23	0.882	4.9	1.12	5.34	0.55	5.90	0.520
300	1.74	0.96	5.5	0.98	6.25	0.75	7.0	0.620
400	2.74	0.98	6.5	0.80	7.15	1.18	8.3	0.733
500	3.72	1.00	7.5	0.68	8.2	1.61	9.8	0.866
600	4.69	1.05	8.4	0.60	9.4	2.03	11.4	1.01
700	5.70	1.08	9.5	0.53	10.8	2.46	13.2	1.16
750	6.22	1.08	9.9	0.51	11.2	2.68	13.9	1.23
800	6.82	1.08	10.4	0.48	11.7	2.95	14.6	1.29
900	7.88	1.08	11.3	0.44	12.7	3.4	16.1	1.42
				Argon				
30	0.012	0.23	2.2	8.6	2.42	0.01	2.43	0.214
40	0.047	0.49	2.5	8.0	5.12	0.02	5.14	0.453
50	0.109	0.85	2.9	7.6	8.9	0.05	9.0	0.795
60	0.204	1.05	3.2	7.2	11.0	0.09	11.1	0.981
70	0.349	1.28	3.5	6.8	13.4	0.15	13.6	1.20
80	0.465	1.69	3.8	6.5	17.6	0.20	17.8	1.57
100	0.89	2.88	4.3	6.0	30.0	0.39	30.4	2.69
120	1.52	3.42	4.7	5.7	35.6	0.66	36.3	3.21
150	2.79	4.89	5.3	5.3	51.8	1.2	53.0	4.68
175	4.31	5.40	5.8	4.9	57.8	1.9	59.7	5.29
200	5.62	5.79	6.1	4.7	62.5	2.4	64.9	5.73
225	7.10	6.45	6.5	4.5	71.1	3.1	74.2	6.57
250	9.1	7.14	6.8	4.3	79.3	3.9	83.2	7.36
300	12.8	8.05	7.4	4.0	91.8	5.5	97.3	8.60
350	17.3	9.11	8.0	3.7	107.0	7.5	115.0	10.2
400	22.0	9.93	8.4	3.5	119.0	9.5	128.0	11.3
450	27.0	10.3	8.8	3.3	126.0	11.7	138.0	12.2
500	31.9	10.5	9.2	3.2	130.0	13.8	144.0	12.8
				Krypton				
40	0.001	0.015	3.2	19.3	0.34	0.001	0.34	0.030
50	0.0034	0.038	3.6	19.6	0.88	0.002	0.88	0.078
60	0.0079	0.057	3.9	19.6	1.34	0.003	1.34	0.120
70	0.0146	0.069	4.3	19.5	1.64	0.006	1.65	0.145
80	0.0228	0.089	4.6	19.3	2.13	0.01	2.14	0.187
				Xenon				
50	0.008	0.008	3.2	24.9	0.225	0.0003	0.225	0.020
60	0.020	0.019	3.5	25.5	0.55	0.001	0.55	0.049
70	0.046	0.030	3.8	26.2	0.90	0.002	0.90	0.079
80	0.084	0.042	4.1	26.9	1.30	0.003	1.30	0.115

[a] Data taken using N_2^+.

[b] Data taken using O_2^+.

[c] Data taken using Ne^{++}.

spectrometers[18,19] were made at 80- and 500-keV Ar^+ bombarding energy, and at the lower bombarding energy there was evidence of a weak component of energy ~ 250 eV that could have been such a shifted argon x ray. The contribution to the measured carbon K x-ray yield at 80 keV is estimated to be less than 20%, and no correction for this effect was made to the data. It was noted during the spectroscopic measurements that during a lengthy argon bombardment of a carbon target, argon buildup in the target led to a steady increase in argon x-ray intensity due to Ar^+-Ar collisions. For this and other reasons related to target surface contamination, fresh target spots and short bombardments with low beam currents were used whenever possible for each data point. The energy-shift effects described above for argon L x rays are fortunately not expected to be important for carbon K x rays, except, perhaps, for x rays originating in the projectile in the C^+-C system. Calculations by House[20] indicate that carbon atoms with both 1s and 2s vacancies can yield K x rays with energies above the ground-state K edge of carbon; such x rays would not be detected in our measurements. Carbon target atoms residing in a solid should, however, have L-shell vacancies filled before K x-ray emission, so in our work x rays from target atoms would probably not be affected. Projectile ions, on the other hand, experience multiple collisions and less recombination, and thus are more likely to emit K x rays from configurations involving outer-shell excitation and ionization. These outer-shell effects influence fluorescence yields as well as x-ray transmission through counter windows, and thus the x-ray contributions from the carbon projectiles are very difficult to estimate. No correction has been made to the C^+-C data for x rays from the projectiles except in a comparison with theory in the following section; for that comparison the measured C^+-C cross sections were arbitrarily divided by 2 (i.e., it was assumed that both target atom and projectile ion contributed equally to the carbon x-ray yield).

III. THEORY AND DISCUSSION

The experimental cross sections shown in Fig. 2 are several orders of magnitude larger than the predictions of a model based on a direct Coulomb interaction. (For a comparison of heavy-ion cross sections with the direct-interaction model see Ref. 6.) The inner-shell excitations in these heavy-ion collisions are assumed to occur at level crossings in the dynamic quasimolecule that is formed during the collision. Such a mechanism was proposed by Fano and Lichten,[4] and is discussed in more detail by Lichten.[21] At large ion-atom separations the electronic states of the system are the normal atomic states of the ion and atom. At zero distance of separation, the states of the system are the atomic states of the atom whose atomic number is the sum of the atomic numbers of the collision partners. At intermediate distances, the electronic energy states are quasimolecular states which change as the ion-atom distance of separation varies. As the particles approach one another in these close collisions, the exclusion principle dictates the occupancy of these molecular levels, some of which may cross with higher, unfilled levels. Electron transitions can occur with high probability at these crossings. This "electron promotion" mechanism is important not only for symmetric collisions (e.g., Ar^+-Ar, as discussed by Fano and Lichten[4]) but also for asymmetric collisions in which the energy of the electronic level under consideration matches the energy of some level in the collision partner.[9]

The cross-section data of Fig. 2 fall roughly into three groups: Curves for incident C^+, O^+, and N^+ are similar to one another (recognizing

TABLE II. Fitting parameters for the level-crossing model.

Incident ion	$4\pi\alpha r_x^2$ (10^{-17} cm^2)	y (a.u.)[a]
C^+	4.42	1.15
N^+	4.52	1.04
O^+	4.77	1.30
Ne^+	1.67	1.28
Ar^+	16.6	0.80

[a]1 a.u. of velocity = 2.18×10^8 cm/sec.

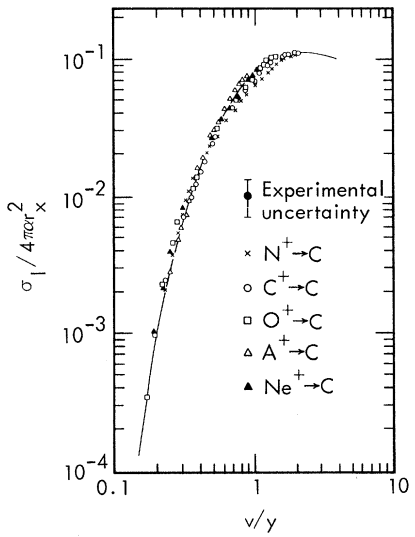

FIG. 3. Comparison of experimental cross sections with predictions of the theoretical model based on Landau-Zener theory. The solid curve represents the theory, and the parameters used in fitting the experimental data are listed in Table II.

TABLE III. Comparison of r_x (assuming $\alpha = 1$) with the sum of the interacting electron-shell radii (Ref. 23).

Incident ion	r_x (Å)	$r_{\text{carbon } K} + r_{\text{projectile}}$ (Å)
C^+	0.187	0.18
N^+	0.190	0.17
O^+	0.195	0.16
Ne^+	0.115	0.15
Ar^+	0.364	0.28

that the C^+ data are high due to x rays from the projectile), the Ne^+ curve is significantly lower, and those for Ar^+, Kr^+, and Xe^+ form a group with much larger cross-section values. These cross-section systematics are consistent with the influences of level matching referred to above and discussed in detail in Refs. 5 and 9. Large cross sections are expected for collisions involving matching, or near matching, of projectile energy levels with the carbon K-shell energy. The Ne^+ cross section is thus low compared to cases involving good K-K level matching (e.g., C^+-C), and the large cross sections for Ar^+, Kr^+, and Xe^+ result because of a good energy match of the carbon K shell with the larger and more complex L, M, and N shells in the projectile ions.

In previous papers[2,3] the authors have shown that cross sections for inner-shell excitation in ion-atom collisions are consistent with a simple theoretical model based on level crossings. This model assumes that the excitation probability at a level crossing follows the form of the Landau-Zener theory.[22] The cross section, based on the assumption of a single level crossing, has the form[2]

$$\sigma = 4\pi\alpha r_x^2 [Q_3(y/v) - Q_3(2y/v)], \quad (3)$$

where

$$Q_n(x) = \int_1^\infty e^{-xt} t^{-n} dt, \quad (4)$$

and where r_x is the level-crossing radius, y is a term in the Landau-Zener theory that depends on the dynamics of the specific level crossing, v is the initial relative velocity of the incident ion, and α is the probability that the appropriate molecular configuration is formed.

In Fig. 3, the cross sections for C^+, N^+, O^+, Ne^+, and Ar^+ are compared with the theoretical model; the plotted points are taken from the experimental data, and the theory is represented by the solid curve. (Note that the C^+-C cross sections were arbitrarily divided by 2 for this comparison in an attempt to correct for x rays from the projectile. The data for Kr^+ and Xe^+ were not considered sufficiently extensive for a meaningful comparison with the theory.) There are two fitting parameters, $4\pi\alpha r_x^2$ and y, which appear as scale factors in Eq. (3). The fitting is very simply accomplished by plotting a curve of experimental cross section as a function of ion velocity on a log-log scale, and then sliding it, to achieve a best fit, over the theoretical curve of Fig. 3 plotted on the same scale. The values thus determined for the fitting parameters are given in Table II.

A lower bound for the level-crossing radius r_x can be obtained by setting $\alpha = 1$. The resulting values suggest that a good estimate for the level-crossing radius is the sum of the radius of the carbon K shell and the radius of the shell in the projectile whose binding energy most closely matches the carbon K-shell binding energy. This correlation is shown in Table III, with the pertinent projectile shell being the K shell for C^+, N^+, O^+, and Ne^+ and the L_I shell for Ar^+.

The relatively low r_x value shown for Ne^+ (for all other projectiles the r_x value exceeds the sum of the pertinent shell radii) may reflect the poor level matching for the Ne^+-C system. This could represent an effect on the actual level-crossing radius *or* a reduction of α, the probability of occurrence of a crossing.

*Work performed under the auspices of the U. S. Atomic Energy Commission.

[1]R. C. Der, T. M. Kavanagh, J. M. Khan, B. P. Curry, and R. J. Fortner, Phys. Rev. Letters 21, 1731 (1968).

[2]R. J. Fortner, B. P. Curry, R. C. Der, T. M. Kavanagh, and J. M. Khan, Phys. Rev. 185, 164 (1969).

[3]R. C. Der, R. J. Fortner, T. M. Kavanagh, and J. M. Khan, Phys. Rev. Letters 24, 1272 (1970).

[4]U. Fano and W. Lichten, Phys. Rev. Letters 14, 627 (1965).

[5]H. J. Specht, Z. Physik 185, 301 (1965).

[6]W. Brandt and R. Laubert, Phys. Rev. Letters 24, 1037 (1970).

[7]F. W. Saris and D. Onderdelinden, Physica 49, 441 (1970); F. W. Saris, *ibid.* (to be published).

[8]P. B. Needham, Jr. and B. D. Sartwell, Phys. Rev. A 2, 27 (1970).

[9]T. M. Kavanagh, M. E. Cunningham, R. C. Der, R. J. Fortner, J. M. Khan, E. J. Zaharis, and J. D. Garcia, Phys. Rev. Letters (to be published).

[10]J. M. Khan, D. L. Potter, and R. D. Worley, Phys. Rev. 139, 1735 (1965).

[11]J. Lindhard, M. Scharff, and H. E. Schiøtt, Kgl. Danske Videnskab. Selskab, Mat.-Fys. Medd. 33, No. 14 (1963).

[12]J. H. Ormrod and H. E. Duckworth, Can. J. Phys. 41, 1424 (1963).

[13]D. I. Porat and K. Ramavataram, Proc. Roy. Soc. (London) A252, 394 (1959).

[14]B. Fastrup, P. Hvelplund, and C. A. Sautter, Kgl. Danske Videnskab. Selskab, Mat.-Fys. Medd. 35, No. 10 (1966).

[15]C. E. Dick and A. C. Lucas, Phys. Rev. A 2, 580

(1970).
[16]W. Whaling, in *Handbuch der Physik*, edited by S. Flügge (Springer-Verlag, Berlin, 1958), Vol. 14, p. 193.
[17]M. E. Cunningham, R. C. Der, R. J. Fortner, T. M. Kavanagh, J. M. Khan, C. B. Layne, E. J. Zaharis, and J. D. Garcia, Phys. Rev. Letters 24, 931 (1970).
[18]R. C. Der, T. A. Boster, M. E. Cunningham, R. J. Fortner, T. M. Kavanagh, and J. M. Khan, Rev. Sci. Instr. (to be published).
[19]T. A. Boster, R. C. Der, R. J. Fortner, T. M. Kavanagh, and J. M. Khan, Nucl. Instr. Methods (to be published).
[20]L. L. House, Astrophys. J. Suppl. 18, 21 (1969).
[21]W. Lichten, Phys. Rev. 164, 131 (1967).
[22]L. Landau, Physik. Z. Sowjetunion 2, 46 (1932); C. Zener, Proc. Roy. Soc. (London) A137, 696 (1932).
[23]J. C. Slater, *Quantum Theory of Atomic Structure* (McGraw-Hill, New York, 1960), Vol. 1, p. 210.

PHYSICAL REVIEW A VOLUME 4, NUMBER 2 AUGUST 1971

Stopping Power and Energy Straggling for Swift Protons

E. Bonderup and P. Hvelplund
Institute of Physics, University of Aarhus, DK-8000 Aarhus C, Denmark
(Received 22 February 1971)

Calculations and measurements of energy dissipation by protons at energies above ~ 100 keV are presented. The calculations, which make use of a statistical model of the atom, are based on a refinement of a procedure suggested by Lindhard and Scharff. The theoretical section of the present paper is concerned with energy straggling, as stopping powers were dealt with in an earlier publication. Measurements of stopping power and energy straggling for 100–500-keV protons have been made in various gases, viz. hydrogen, helium, air, neon, argon, and krypton. The stopping-power data are in good agreement with theory and earlier experimental work. For the heavy gases, the experimental straggling values are seen to be an increasing function of energy, as expected from theory. In a more quantitative comparison, however, some discrepancy between theory and experiment is observed.

I. INTRODUCTION

Consider a beam of heavy particles of low charge number traversing matter. The average energy loss is a quantity of great interest, and it has been studied extensively, both theoretically and experimentally. Sometimes, however, it becomes necessary to pay attention to the fact that during penetration, the energy distribution of the beam is broadened. This happens because slowing down is the result of individual collision events, the number of which is governed by statistical laws.

In the following we present a theoretical and experimental investigation of straggling, i.e., the mean-square deviation in energy loss. For a sufficiently fast particle, only collisions with electrons contribute appreciably to the slowing-down (electronic stopping, Sec. IV B). Only such cases will be treated below. On the other hand, we concentrate on such low energies that a well-known asymptotic expression for straggling does not apply.

II. THEORY

A general discussion of energy loss has been given by Bohr.[1] For the straggling Ω^2, one obtains in limiting cases

$$\Omega^2 = \Omega_B^2 = 4\pi Z_1^2 Z_2 e^4 N \Delta R \ , \qquad (1)$$

where $-e$ is the charge of the electron, Z_1 and Z_2, the atomic numbers of the projectile and the target atoms, respectively, N the number of atoms per unit volume, and ΔR the target thickness. The above expression is derived under the following conditions: (i) The target atoms are randomly distributed; (ii) the velocity of the projectile is high as compared to the orbital velocities of the target electrons; (iii) the energy of the projectile is changed only slightly during penetration. In the following, conditions (i) and (iii) will always be assumed to be fulfilled.

If, for some of the electrons, condition (ii) is not satisfied, a calculation of average energy loss and straggling becomes rather complicated. A fairly simple treatment of cases, where condition (ii) is not necessarily fulfilled, was suggested by Lindhard and Scharff and found to be useful.[2,3] The idea was to use, as far as possible, a comparison with an electron gas of constant density, for which exact results can be obtained. Such a treatment is of Thomas-Fermi type and thus contains the kind of similarity which is characteristic for a Thomas-Fermi description.

In the case where a heavy nonrelativistic particle of charge $Z_1 e$ and velocity v only exerts a perturbing influence on a free electron gas of density ρ, all quantities connected with the slowing down of the particle can be expressed in terms of the longitudinal dielectric constant $\epsilon^l(k, \omega)$ for the gas.